RESERVOIR INDUCED SEISMICITY—A NEW MODEL

S. K. SAXENA,* A. METIN GER† AND A. SENGUPTA‡

Department of Civil Engineering, Illinois Institute of Technology, Chicago, IL 60616, U.S.A.

SUMMARY

Deficiencies of different existing models on 'Reservoir Induced Seismicity' have been discussed and a new mathematical model, which enhances a better understanding of triggering mechanism in terms of changes in effective stresses, *in situ* stresses and water level variations, has been discussed in this paper. In the model fractured rock is simulated by a fluid-filled elastic material subject to Mohr–Coulomb failure criterion. The model has been found to be capable of responding effectively to site specific attributes. It can recognize and explain the phenomenon of time lag observed in several actual cases. It is also capable of simulating stabilization of rock–reservoir system after a period of activities that follow the initial stage of filling. One dimensional and two dimensional, isotropic and anisotropic cases have been analysed and the model predictions have been found to agree qualitatively with the field observations.

INTRODUCTION

The seismicity induced by the filling of and/or variations in the level of water impounded by large reservoirs (herein after called RIS) is considered as an increasingly recognized threat. There are quite a number of cases of RIS reported worldwide (a partial list of such occurrences is given in Reference 1). Comprehensive examination of these cases revealed that RIS often is associated in space and in time with water level fluctuations, the filling history (FH) of the reservoir. A statistical model, based on the reported correlations between FH and RIS only, is far from producing explanatory and predictive representation of triggering mechanisms of RIS activities. This is mostly due to the dependence of such occurrences on site-specific discriminating attributes. In addition to statistical studies,[2–6] there are a number of theoretical attempts made to explain the triggering mechanism of RIS. Models of elastic half-space[7–10] and models of elastic fluid-filled materials[11–13] have been applied to RIS cases.

Models of elastic half-space proved that the magnitude of shear stress created even by the deepest reservoirs is of an order of magnitude too small to initiate a movement. Furthermore, these models failed to explain why a delay occurs between water level fluctuations and the detected seismicity and why the seismicity does not always occur immediately after initial filling. The deficiency of the elastic half-space models led to the development of the models of elastic fluid-filled materials. In these models, effective stress was considered as the triggering mechanism of RIS activities. This approach allowed much larger stresses to be generated at depth, but failed to explain why the changes in water level in the reservoir triggers RIS in a few but not all cases.

A comparative evaluation of reported induced seismicity and reassessment of the available

---

* Professor and Chairman.
† Associate Professor.
‡ Research Assistant.

mathematical models suggests that the triggering mechanism of RIS activities may be explained more thoroughly knowing both the *in situ* state of stress and the changes in the effective stresses induced by water level variations in the reservoir.[14,15] In this paper, an assessment of a mathematical model which enhances a better understanding of the triggering mechanism in terms of changes in effective stress, *in situ* stress, and the water level variations, is presented.

THE MATHEMATICAL MODEL

In the model, fractured rock is simulated by a fluid-filled elastic material subject to the Mohr–Coulomb failure criterion. According to this criterion, materials fail when shear stress on the failure plane, at failure, reaches some unique function of the normal stress on that plane. The unique function is known as the failure envelope.

The sign convention adopted in this study is such that the compressive stress and the extensive strain are positive.

For an idealized rock–reservoir system of Figure 1, the major principal stress (σ_z; vertical stress) is equal to the overburden pressure. It is further assumed that the coefficient of earth pressure at rest, K_0, varies in a statistically homogeneous random fashion in order to provide a better simulation of the *in situ* state of stress. Considering the fact that reservoirs are rather extensive in area, the fractured rock can be assumed not to deform laterally. Combining this observation with the experimental evidence that fractures deform linearly with increasing effective stress, as reported by Snow,[16,17] the change in effective principal stresses, $\Delta\bar{\sigma}_x$, $\Delta\bar{\sigma}_y$ and $\Delta\bar{\sigma}_z$, may be shown to be a function of loading pattern and corresponding change, u, of the pore pressure:

$$\Delta\bar{\sigma}_x = \frac{A_x}{E}[v\Delta\sigma_z - (1-v)u] \tag{1a}$$

$$\Delta\bar{\sigma}_y = \frac{A_y}{E}[v\Delta\sigma_z - (1-v)u] \tag{1b}$$

$$\Delta\bar{\sigma}_z = \Delta\sigma_z - u \tag{1c}$$
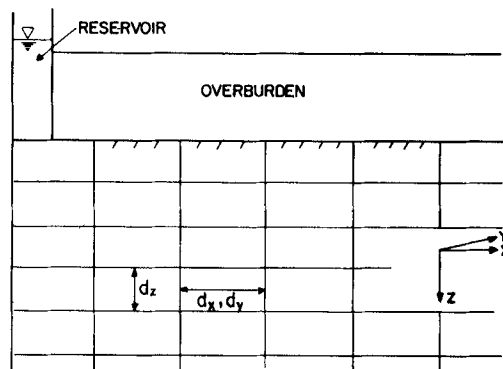

Figure 1. Idealized rock–reservoir system

where

$$A_x = \frac{(1+v)/E - 1/(G_y d_y)}{[1/E - 1/(G_x d_x)][1/E - 1/(G_y d_y)] - v^2/E^2} \tag{1d}$$

$$A_y = \frac{(1+v)/E - 1/(G_x d_x)}{[1/E - 1/(G_x d_x)][1/E - 1/(G_y d_y)] - v^2/E^2} \tag{1e}$$

and v is the Poisson's ratio, E is the modulus of elasticity, G_x and G_y are the stiffnesses of rock inclusive of fractures, and d_x and d_y are the average representative distances between fractures, in x and y directions, respectively.

The ratio of principal effective stress increments can then be evaluated to assess the likelihood of failure, i.e. triggering. However, this evaluation cannot be implemented unless u, the change in pore pressure, is known.

To evaluate pore pressures, the seepage into rock must be determined. For an element shown in Figure 2 within the soil, the water mass balance can be expressed as

$$-\left(\frac{\partial \rho V_x}{\partial x} + \frac{\partial \rho V_y}{\partial y} + \frac{\partial \rho V_z}{\partial z}\right)\Delta V = \frac{\partial(\rho \Delta V_W)}{\partial t} \tag{2}$$

where V_x, V_y and V_z are the components of seepage velocity, in x, y and z directions, respectively, and ΔV is the volume of the element, ΔV_w is the volume of the water within the element (since fully saturated, it is the volume of voids), and ρ is the mass density of water. The right-hand side of equation (2) can be expanded:

$$\frac{\partial(\rho \Delta V_W)}{\partial t} = \rho \frac{\partial(\Delta V_W)}{\partial t} + \Delta V_W \frac{\partial \rho}{\partial t} \tag{3}$$

with

$$\partial(\Delta V_W) = \partial(n_x \Delta x)\Delta y \Delta z + \partial(n_y \Delta y)\Delta z \Delta x + \partial(n_z \Delta z)\Delta x \Delta y$$

where, n_x, n_y and n_z are the linear porosities that define the ratio of average fracture aperture to the average distance between the fractures in x, y and z directions, respectively. Using the compatibility conditions that the net lateral strain should vanish, the change in volume of water can be shown to be

$$\partial(\Delta V_W) = \left(\frac{\Delta \bar{\sigma}_x}{G_x d_x} + \frac{\Delta \bar{\sigma}_y}{G_y d_y} - \frac{\Delta \bar{\sigma}_z}{G_z d_z}\right)\Delta V \tag{4}$$
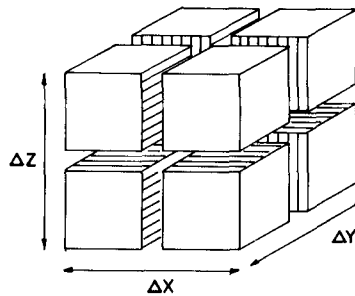

Figure 2. Rock element

Furthermore,

$$\partial\rho = \rho\beta\partial P \tag{5}$$

where β = compressibility of water. Hence, combining equations (2), (4) and (5), the mass balance can be represented by the following equation:

$$-\nabla\cdot(\rho q) = \frac{\rho}{G_x d_x}\frac{\partial\Delta\bar{\sigma}_x}{\partial t} + \frac{\rho}{G_y d_y}\frac{\partial\Delta\bar{\sigma}_y}{\partial t} - \frac{\rho}{G_z d_z}\frac{\partial\Delta\bar{\sigma}_z}{\partial t} + n_T\rho\beta\frac{\partial P}{\partial t} \tag{6}$$

where q = velocity vector and n_T = the total porosity = $V_w/\Delta V$.

The left-hand side of equation (6) can be transformed by using Darcy's law (as shown in Reference 18), to:

$$-\nabla\cdot(\rho q) = \rho\left[\frac{\partial}{\partial x}\left(\frac{k_x}{\gamma}\frac{\partial P}{\partial x}\right) + \frac{\partial}{\partial y}\left(\frac{k_y}{\gamma}\frac{\partial P}{\partial y}\right) + \frac{\partial}{\partial z}\left(\frac{k_z}{\gamma}\frac{\partial P}{\partial z}\right) - 2\beta k_z\frac{\partial P}{\partial z}\right] \tag{7}$$

where k_x, k_y and k_z are the average permeabilities in x, y and z directions, respectively, and γ is the unit weight of water. Incorporating equations (1), (7) and the following relationship between the porepressure u and total pressure P

$$P = \gamma z + u \tag{8}$$

into equation (6) and then rearranging, one obtains

$$\frac{\partial}{\partial x}\left(k_x\frac{\partial P}{\partial x}\right) + \frac{\partial}{\partial y}\left(k_y\frac{\partial P}{\partial y}\right) + \frac{\partial}{\partial z}\left(k_z\frac{\partial P}{\partial z}\right) - 2\gamma\beta k_z\frac{\partial P}{\partial z} =$$

$$\gamma\left\{n_T\beta - \frac{A_x(1-v)}{EG_x d_x} - \frac{A_y(1-v)}{EG_y d_y} + \frac{1}{G_z d_z}\right\}\frac{\partial P}{\partial t}$$

$$-\gamma\left[-\frac{vA_x}{EG_x d_x} - \frac{vA_y}{EG_y d_y} + \frac{1}{G_z d_z}\right]\frac{\partial\Delta\bar{\sigma}_z}{\partial t} \tag{9}$$

The terms in the second bracket on the right-hand side of equation (9) represents the change in volume of fluid within the soil element under a unit change in pressure and will be called S^*, a storativity coefficient for fractured rock. The terms in the third bracket on the right-hand side of the same equation, on the other hand, represents the change of volume under unit load; it is a representative global compressibility of the fractured rock and will be called α. Hence, the mass balance equation becomes

$$\frac{\partial}{\partial x}\left(k_x\frac{\partial P}{\partial x}\right) + \frac{\partial}{\partial y}\left(k_y\frac{\partial P}{\partial y}\right) + \frac{\partial}{\partial z}\left(k_z\frac{\partial P}{\partial z}\right) - 2\beta\gamma k_z\frac{\partial P}{\partial z} = \gamma S^*\frac{\partial P}{\partial t} - \gamma\alpha\frac{\partial\Delta\bar{\sigma}_z}{\partial t} \tag{10}$$

where the change in the major principal stress, $\Delta\bar{\sigma}_z$, can be related to the load $H(t)$, the water level in the reservoir FH, as

$$\Delta\bar{\sigma}_z = I\gamma H(t) \tag{11}$$

where I is the influence factor.[19]

A numerical integration approach is attempted to solve equation (10). In case of an infinitely large reservoir area and a homogeneous-isotropic rock, the flow equation reduces into an integrable form:

$$\frac{\partial^2 P}{\partial z^2} - 2\gamma\beta\frac{\partial P}{\partial z} = \frac{\gamma S^*}{k_z}\left(\frac{\partial P}{\partial t} - \frac{\gamma\alpha}{S^*}\frac{\partial H}{\partial t}\right) \tag{12}$$

subject to

$$P = \gamma z \qquad\qquad t \leq 0 \tag{13a}$$

$$P = \gamma(z + H) \qquad z = 0 \tag{13b}$$

As shown in Reference 20, a solution of the following form exists:

$$P = \gamma z + \gamma H(t) \qquad \left(z < \frac{A}{B} t \right)$$

$$P = \gamma z + \gamma \left(1 - \frac{\alpha}{S^*} \right) \frac{2}{\sqrt{\pi}} \int_\eta^\infty H \left[t - \frac{\left(z - \frac{At}{B} \right)^2}{4\xi^2/B} \right] \cdot e^{\xi^2} d\xi + \frac{\gamma\alpha}{S^*} H(t) \tag{14}$$

$$\left(\frac{A}{B} t < z \right)$$

where

$$A = 2\beta\gamma$$

$$B = \gamma S^*/k_z$$

$$\eta = (z - At/B)/2(t/B)^{0.5} \tag{15}$$

For a two-dimensional problem, equation (10) reduces to

$$\frac{\partial}{\partial x}\left(\frac{k_x}{\gamma} \frac{\partial P}{\partial x} \right) + \frac{\partial}{\partial z}\left(\frac{k_z}{\gamma} \frac{\partial P}{\partial z} \right) - 2\beta k_z \frac{\partial P}{\partial z} - S^* \frac{\partial P}{\partial t} + \alpha \frac{\partial \Delta\bar{\sigma}_z}{\partial t} = 0 \tag{16}$$

Integration of equation (10) will give the variation in u, the change in the pore pressure, within the rock mass subject to a specified FH.

Assuming a linear failure envelope for the state of stress to be in a failure-free zone, the ratio, R, of the effective principal stresses $\bar{\sigma}_z$ and $\bar{\sigma}_x$ should satisfy the following condition

$$R = \frac{\bar{\sigma}_x}{\bar{\sigma}_z} > \frac{1 - \sin\phi}{1 + \sin\phi} \tag{17}$$

where, ϕ is the slope of the envelope. However, if R fails to satisfy this condition, then failure is not warranted. Therefore, to determine the likelihood of localized failure, it is imperative to know both an estimate of R and the in situ state of stress.

Once u is known, the ratio R can be evaluated to assess the likelihood of the triggering of RIS. However, the initial state of stress must be known to be able to assure activation of triggering via stress path analysis. It must be clarified here that numbers of RIS activity are simply numbers of likelihood of failure at some point in the rock mass under consideration, determined by the Mohr–Coulomb criteria.

No attempt has been made in this presentation to calculate any energy transmitted during a failure and hence it is currently not possible to tell whether any failure or which failure will lead to an earthquake. It is hoped that such extension will be incorporated in future. The RIS activity as presented in the examples to follow is indeed the number of failures which may or may not lead to earthquakes. Hence in the figures presented in the following section they are termed as relative RIS activity. Furthermore, it is known that each RIS activity, which may be considered as a local failure within the rock mass, is followed by re-establishment of a stable configuration. The model simulates this effect, whenever it recognizes a triggering, by assigning in a random fashion a new value to K_0, at the position of recognized failure, keeping the horizontal effective stress

unchanged. In other words, it is implicit in this implementation that the amount of energy released during the period between the triggering and re-establishment is assumed to be a random entity. The new state of stress thus acquired is, of course, within the failure-free zone.

RESULTS AND DISCUSSION

To demonstrate the compliance of the model predictions with the reported RIS histories, three series of numerical experiments were attempted.

In the first series, a hypothetical site with infinite areal extent is considered. This site with shear modulus, $G = 10^9$ N/m^3 and depth, $d = 6$ m, has a coefficient of lateral pressure at failure, K_f of 0·17, and is essentially homogeneous and isotropic. K_0 is assumed to be statistically homogeneous to have a more realistic representation of the initial state of stress. The reservoir which is also infinitely large in areal extent is represented by three hypothetical FHs as shown in Figure 3. The cases investigated in this series are described in Table I. In Figure 4, predictions of the model in
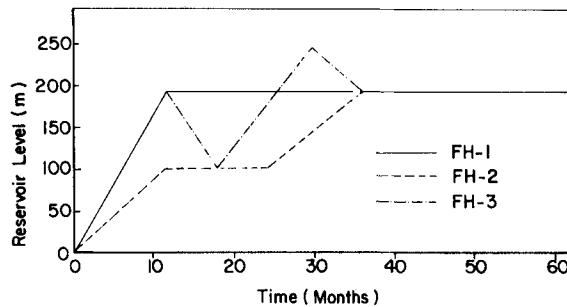
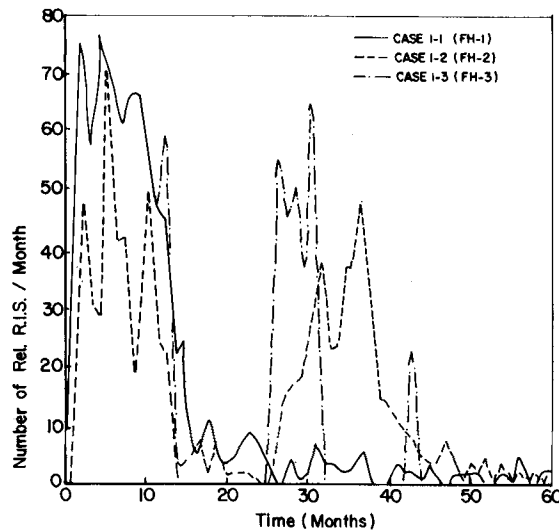Figure 3. Filling histories used in the first series

Figure 4. Comparison of realtive RIS distribution for different FHS

terms of distribution of the number of relative RIS activities triggered per month in the entire
rock mass analysed, under three FHs considered, are shown (cases 1–1, 1–2, 1–3). The examin-
ation of this figure reveals that the majority of relative RIS activities occur during the rising phase
of a FH. However, as also demonstrated in Figure 4, a significant number of triggerings take place
long after variations in reservoir level ceased and/or during a recession phase (the local peaks at
or about the 43rd month correspond to failure at the fault). The delay in some of the triggerings,
as predicted, is due to the dependence of triggering on both FH and the initial state of stress. In
Figure 5, the dependence on the initial state of stress is illustrated. In this figure, five stress paths
under FH-3 at 250 m below the ground level corresponding to five different K_0 values are shown.
During the first year of FH, the rock mass demonstrates a tendency to fail irrespective of the
initial state of stress. However, activation of triggering, i.e. failure, will take place only for two

Table I. Characteristics of the runs in the first series of numerical experiments

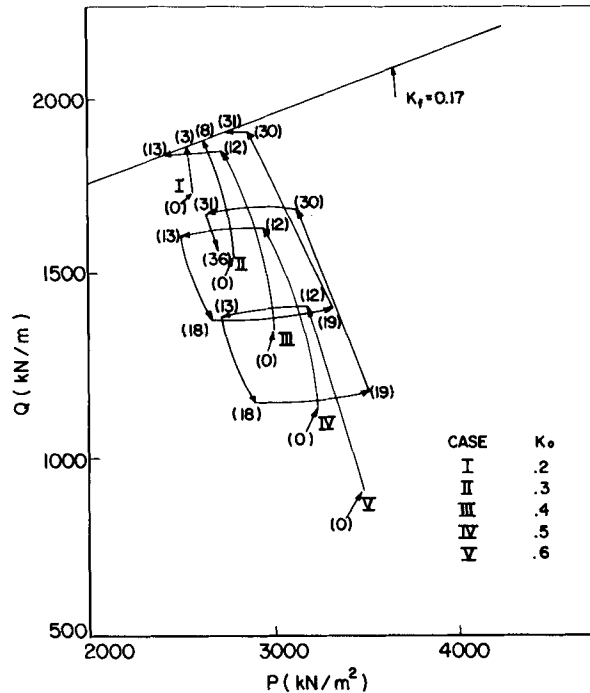| Case no.	FH	Permeability $(10^{-9}$ m/s)	Porosity	Poisson's ratio
1–1	1	0·167	0·1	0·3
1–2	2	0·167	0·1	0·3
1–3	3	0·167	0·1	0·3
1–4	1	0·7	0·3	0·3
1–5	1	1·67	1·0	0·3

Figure 5. Dependence of triggering on initial state of stress (Arabic numerals in parentheses denote months)

cases with K_0 of 0·2 and 0·3 during the first year. For K_0 of 0·4, triggering will be activated within the 13th month during which water level is decreasing. For K_0 of 0·5, activation of triggering is further delayed to take place during the 31st month, the second recession phase. For K_0 of 0·6, triggering will not be activated at all. In other words, depending upon the initial state of stress, relative RIS activity may be activated with no delay or with some delay or not activated at all; the model is capable of assessing the tendency for triggering as well as capable of recognizing a failure.

Figure 6 demonstrates the dependence of number of relative RIS activities on the FH. In this figure, the cumulative number of relative RIS activities under three FHs are shown. The model predicts a larger number of activities during the first year of filling for FH-1 and FH-3, for which the rate of rise of reservoir level is 200 m/yr, than for FH-2 for which the water level rises at 100 m/yr rate. Furthermore, at the end of a 60 months observation period, the greatest total number of activities belongs to FH-3 which contains the deepest reservoir level of 250 m. These predictions of the model are in agreement with reported field histories of RIS activities.[1,4,5] Figure 6 further demonstrates that the reservoir–rock system is stabilized after a period of activities that follow initial filling stage. This agrees with the reported observations.[1,4,5] After an active period of 10–12 years following the stabilization of water level, a reservoir starts to behave like a natural lake, i.e. no relative RIS can be observed after 10–12 years.

The effect of permeability/porosity on the relative RIS activities is demonstrated in Figure 7. In this figure, cumulative number of relative RIS activities for cases 1–1, 1–4 and 1–5 are plotted. With decreasing permeability, time of stabilization for the same FH becomes longer. This time-delay effect of permeability exhibited by the model is in agreement with the observation made on the influence of permeability by Packer et al.[1]

In the second series, a two-dimensional rectangular reservoir of width 40 m is considered. It is assumed that the reservoir site is symmetric about the reservoir centreline. The fully saturated rock mass is fractured in both horizontal and vertical directions. The centre-to-centre distance between the horizontal fractures is 50 m. For the vertical fractures, the centre-to-centre distance is 40 m, except in the zone between 880 m and 1320 m from the centreline of the reservoir where it is 20 m. The lower boundary of the rock at 250 m below the bottom of the reservoir is assumed to be impervious. The lateral extent of the rock mass is limited to 1600 m from the centreline of the reservoir. At 1600 m, the side boundary is assumed to be sufficiently away from the reservoir so
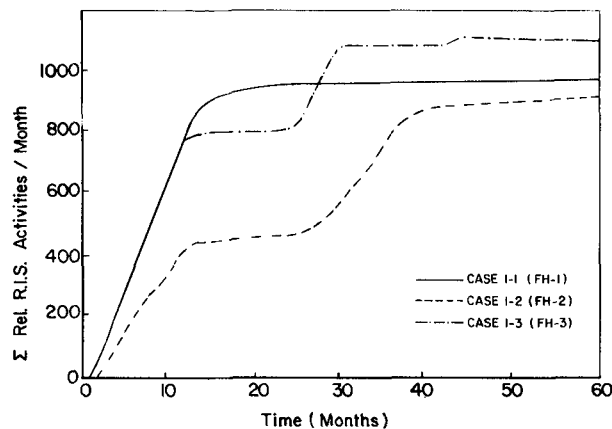

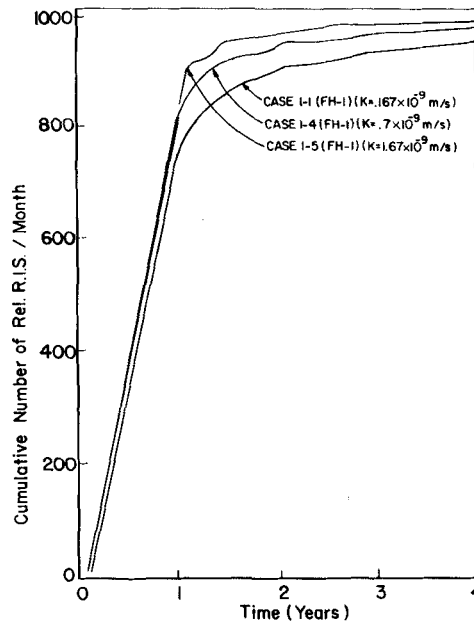Figure 6. Cumulative distribution of relative RIS activities

Figure 7. Time delay effect of permeability
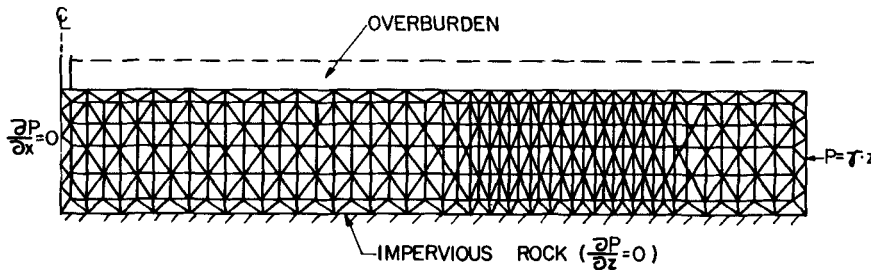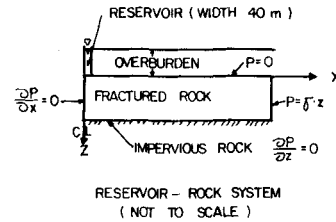

RESERVOIR – ROCK SYSTEM
(NOT TO SCALE)

Figure 8. The finite element mesh

that reservoir effect on the prevailing hydrostatic pressure distribution cannot be felt. Similar to the first series, the rock mass is assumed to be isotropic and homogeneous, except for K_0 which is assumed to be statistically homogeneous. There is also an overburden of uniform thickness of 150 m over the rock mass. The schematic of the rock–reservoir system and the boundary conditions are shown in Figure 8.

Figure 8 also illustrates the nodes and the finite element mesh used in this study. The total

integration span was 5 years. The time increment, based on convergence and accuracy consider-
ations, was selected to be 1 month. The total stress increments (equation 11), at the nodes
resulting from water level changes within the reservoir were determined using the Boussinesq
solution.[19]. In other words, the reservoir load was treated as a single point load acting through its
centre of gravity. This assumption will remain valid as long as the width of the reservoir is much
smaller than the vertical and lateral extent of the integration domain, except at the node just
beneath the reservoir.

In this series, the effects of permeability or hydraulic conductivity, k, and several mechanical
properties such as the intercept of the failure envelope, T_s, slope of the failure envelope, ϕ, and the
stiffness of rock inclusive of fractures, G, were examined. The hypothetical FH used in this series
of runs is shown in Figure 9. The cases studied in this series are described in Table II.

The effect of permeability or hydraulic conductivity on the temporal distribution of relative
RIS as predicted by the model is shown in Figure 10. It has been found that for a lower value of
permeability the maximum number of relative RIS per month remains low at the initial stage, but
it continues long after the stabilization of the water level of the reservoir. For higher values of
permeabilities, the model predicts a higher number of relative RIS activities during the period of
initial rise of the water level in the reservoir; but it ceases shortly after the stabilization of the
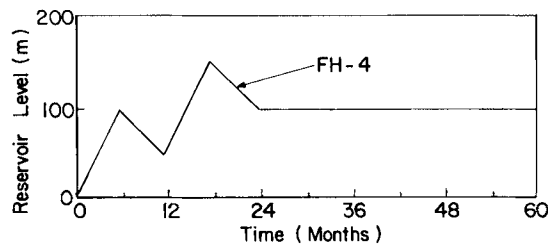

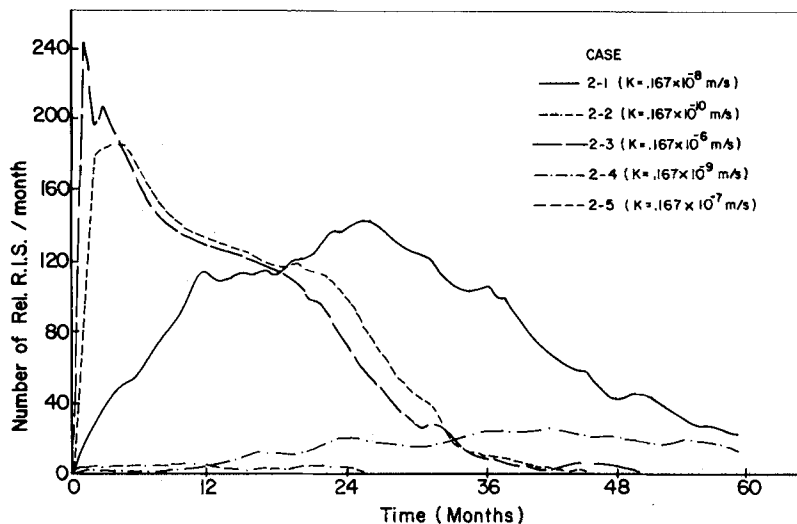Figure 9. Filling history used in the second series

Figure 10. Effect of permeability on the temporal distribution of RIS

Table II. Characteristics of the runs in the second series of numerical experiments (T_s = intercept of the failure envelope; ϕ = slope of the failure envelope)

Case no.	$G_x(10^6$ Pa/m)	$G_y(10^6$ Pa/m)	$k(10^{-8}$ m/s)	T_s(MPa)	ϕ(degrees)
2–1	1	0·1	0·167	0·5	15
2–2	1	0·1	0·00167	0·5	15
2–3	1	0·1	16·7	0·5	15
2–4	1	0·1	0·0167	0·5	15
2–5	1	0·1	1·67	0·5	15
2–6	1	0·1	0·167	1·0	15
2–7	1	0·1	0·167	0·1	15
2–8	1	0·1	0·167	0·5	22·5
2–9	1	0·1	0·167	0·5	30·0
2–10	0·8	0·08	0·167	0·5	15
2–11	1·1	0·11	0·167	0·5	15

water level in the reservoir. So, as permeability gets smaller, a larger delay is predicted for the maximum numbers of relative RIS per month, herein called maximum frequency of relative RIS. This time lag is due to the dependency of seepage velocity on permeability.

Howells[21] has used a one-dimensional diffusion equation assuring uniform rock properties in calculating the time required for a substantial rise in pore pressures at different depths. Interestingly he arrived at similar conclusion, that the time required for a pore pressure development at any depth to trigger a RIS is a function of the permeability of that region.

Large seepage velocities corresponding to large permeabilities transmit the pressure changes due to water level fluctuations at faster speeds than the small seepage velocities of low permeabilities. Furthermore, small permeabilities imply greater resistance to seepage. In other words, with decreasing permeability the magnitude of change in pressure should decay more rapidly with increasing distance from the reservoir. That is to say, with decreasing permeability the total number of occurrences of relative RIS activities should decrease. In the limiting case, with an impervious rock, there would be no relative RIS activity triggering, as suggested by elastic half-space models.[7-10] The model is also capable of simulating this effect.

Figure 11 shows the variation of total number of relative RIS with permeability. Figure 12 shows the variation of cumulative number of RIS with permeability. As has been discussed above and can be clearly inferred from Figures 11 and 12, a range of intermediate values of permeabilities (around 10^{-8} m/s) can be defined for which the seepage velocity will not be large enough to trigger RIS instantaneously, due to larger time lag, but will cause large pressure build-up—large enough to trigger the maximum number of relative RIS. This value appears to be a threshold and for any permeability above or below, the cumulative number of relative RIS will be less. If the permeability of the rock mass is larger than the threshold, the seepage velocity being relatively high will cause less pressure build-up. So, although the time lag between the impoundment of the reservoir and the maximum frequency of relative RIS will be smaller, yet the total number of relative RIS will not reach the peak value. Conversely, if the permeability of the medium is smaller than the threshold, the seepage velocity will be smaller causing longer time lag, and at the same time pressure build-up at some remote point of the system will cause failure of rock mass even after stabilization of the reservoir water. This explains the peak observed in Figure 11 for an intermediate or threshold value of the permeability of the medium.

The adopted failure criterion suggests that with increasing tensile strength, T_s, and/or the slope
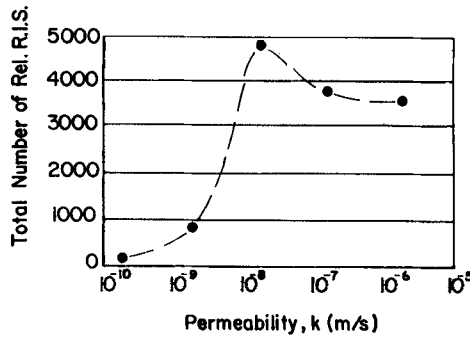
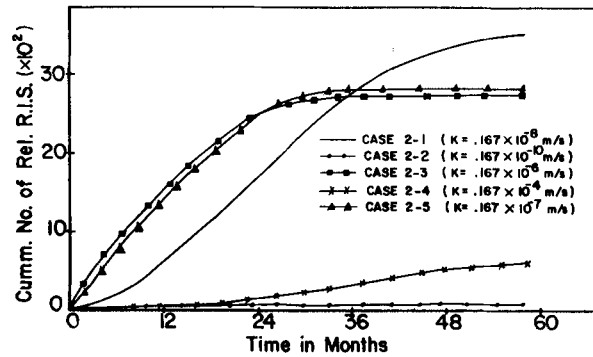Figure 11. Effect of permeability on total number of relative RIS

Figure 12. Effect of permeability on the cumulative number of relative RIS occurrences

of the failure envelope, ϕ, the fractured rock becomes increasingly less prone to relative RIS activities. This is due to the expansion of failure free zone, as shown in Figure 13, with increasing T_s, and/or ϕ. The model, as demonstrated in Figures 14 and 15, is perfectly capable of simulating this implication of the adopted failure criterion.

The effect of stiffness of rock, inclusive of fracture, G, on the distribution of RIS activities is shown in Figure 16. The model predicts a decrease in both the frequency of occurrences and the total number of occurrences of relative RIS activities with increasing stiffness. This predicted dependence is in good agreement with the expected response. The larger the stiffness (i.e. smaller deformations), the smaller will be the changes in effective stresses. In other words, under the same load there is less likelihood of triggering of relative RIS activities to occur for larger stiffness.

In the third series, sensitivity of the model to several site-specific attributes such as filling history, shape of the reservoir, anisotropy and heterogeneity are examined. All of the geometric characteristics of the rock mass are the same as that of the second series. However, similar to K_0 values, permeability is assumed to be statistically homogeneous. The characteristics of the runs in this series are given in Table III. The two hypothetical FHs used in this series are shown in Figure 17.

The three different shapes of the reservoir considered are shown in Figure 18 as section-1 (narrow rectangular channel section), section-2 (wider rectangular channel section) and section-3
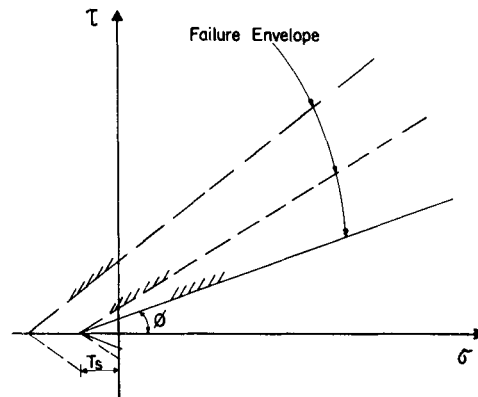
Figure 13. Failure criterion and its effect on the extent on failure-free zone
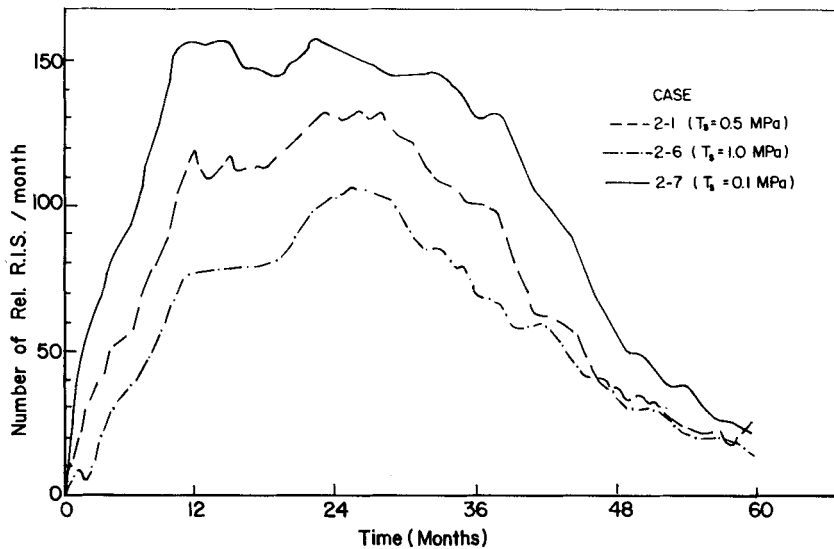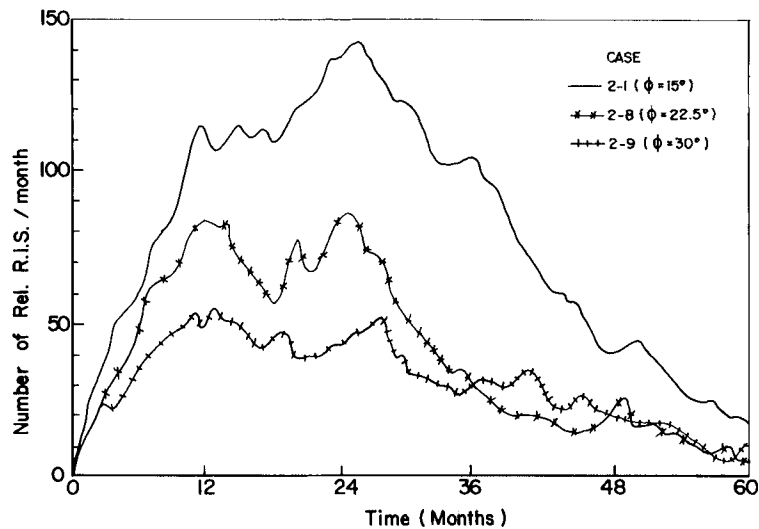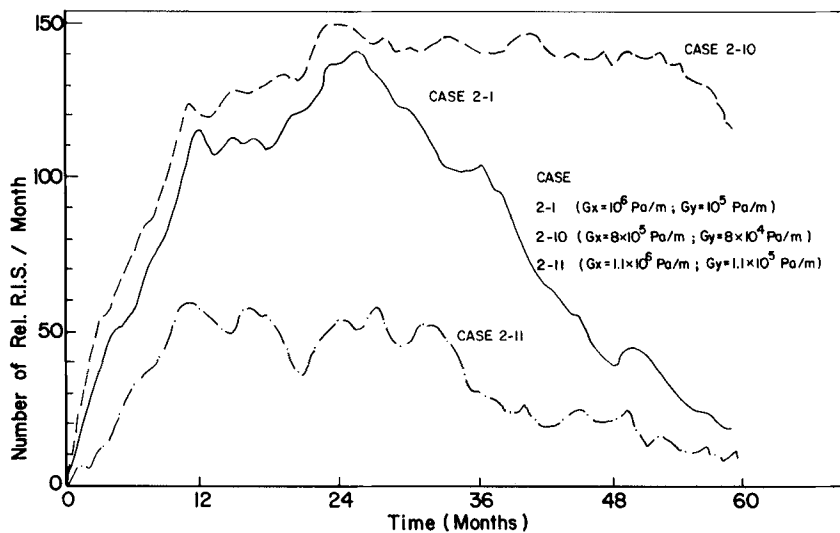

Figure 14. Effect of T_s on the number of occurrences of relative RIS activities

(trapezoidal channel section). The reservoir is assumed to be symmetric about its centreline, so only one-half of the reservoir cross-section is shown in the figure. The model, which is sensitive to FH, fails to demonstrate any discernible dependence on the shape of the reservoir cross-section, as illustrated in Figure 18. This may be attributed to the fact that the two-dimensional mathematical model lacks the capability of simulating the areal extent and/or volume of the reservoir, two significant parameters shown by statistical models[2-6] to be correlated to relative RIS activities.

Anisotropy and heterogeneity are too site-specific to discern any general trends as to how they affect relative RIS. In the following, the predictions of the model for some anisotropic or heterogeneous cases are presented to demonstrate the sensitivity of the model to such site-specific attributes.

Figure 15. Effect of ϕ on the number of occurrences of relative RIS activities

Figure 16. Effect of G on the number of occurrences of relative RIS activities

Two anisotropic and statistically homogeneous cases, with the ratio of mean permeabilities in vertical and horizontal directions of 0·1 and 10, are considered. Compared in Figures 19 and 20 are the model predictions for these anisotropic cases and the isotropic case. As is illustrated in Figure 19, the activities in the case of higher vertical permeability cease as soon as the reservoir water level is stabilized, while in the case of higher horizontal permeability they continue to occur long after the stabilization. This can be attributed to the small depth-lateral extent ratio of the site, which in the case of high vertical permeability enables the pressure field to reach equilibrium

Table III. Characteristics of the runs in the third series of numerical experiments

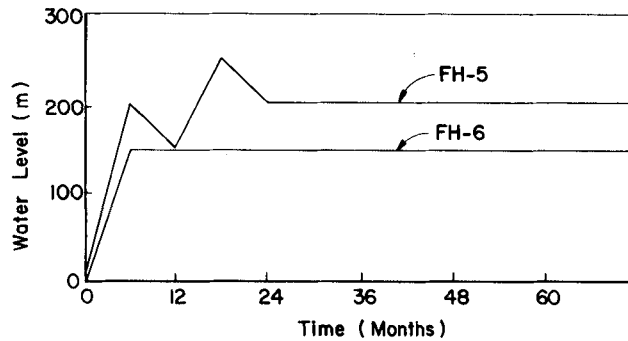| Case no.	$k_x \times 10^{-8}$ (m/s)	k_z/k_x	FH	Reservoir section	Heterogeneity
3–1	0·525–5·25	1·0	5	1	None
3–2	0·525–5·25	1·0	6	1	None
3–3	0·525–5·25	1.0	5	2	None
3–4	0·525–5·25	1·0	5	3	None
3–5	5·25–52·5	0·1	5	1	None
3–6	0·525–5·25	10·0	5	1	None
3–7	See Figure 22	N.A.	5	1	Permeable zone
3–8	0·525–5·25	1·0	5	1	N-fault
3–9	0·525–5·25	1·0	5	1	F-fault

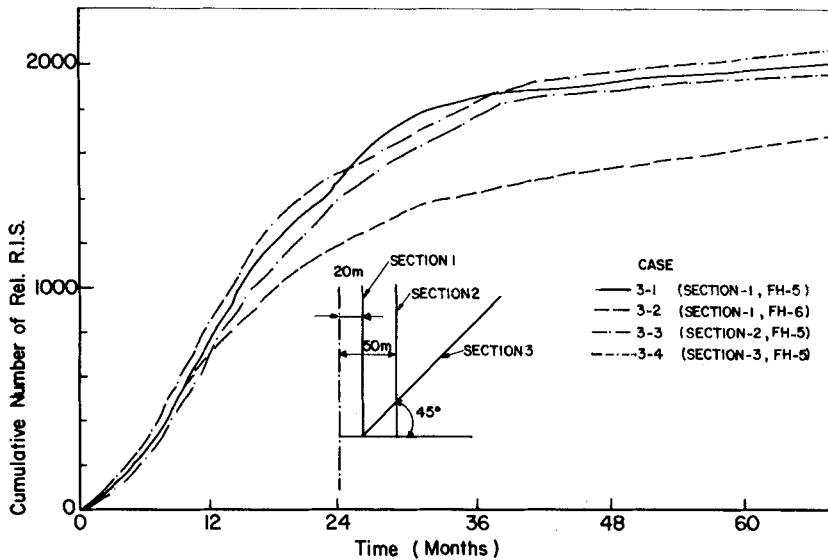Figure 17. Filling history used in the third series

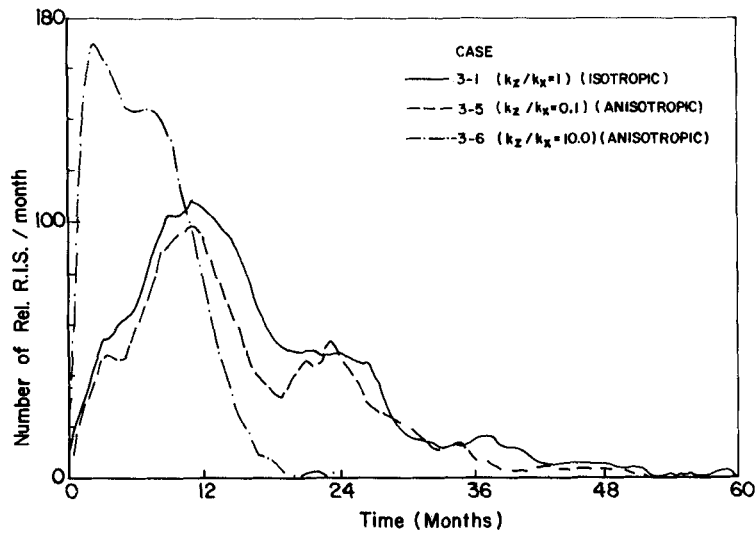Figure 18. Effect of reservoir shape and filling history
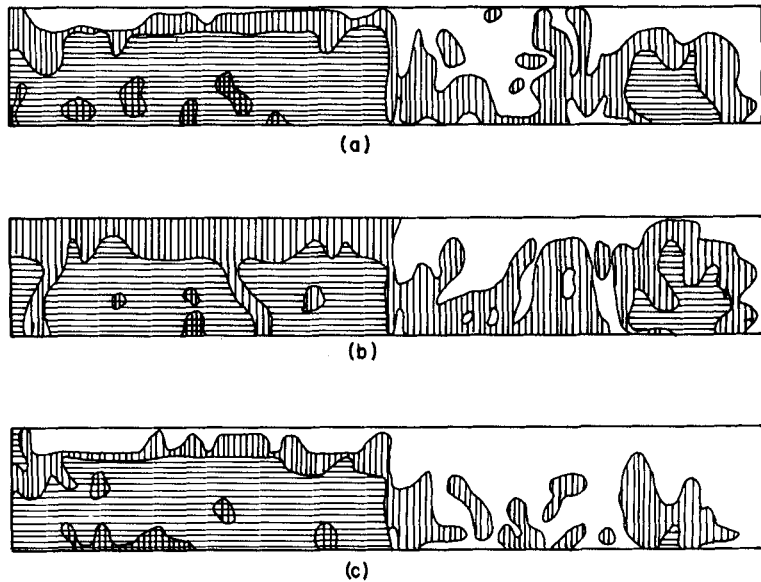
Figure 19. Effect of anisotropy

Figure 20. Spatial distribution of total number of relative RIS activities during first 60 months period: (a) isotropic case, and anisotropic cases of (b) $k_z/k_x = 0.1$ and (c) $k_z/k_x = 10.0$ (⬚ 0   RIS; ⬚⬚⬚⬚⬚⬚ 1–10 activities; ▤▤ 11–20 activities; ▦▦▦▦▦ 21–40 activities; ■■■■ >40 activities)

at the same time as the reservoir water level is stabilized. Moreover, as shown in Figure 20, with higher permeability in the vertical direction, activities are mostly confined to a region closer to the reservoir, whereas with higher permeability in the horizontal direction, they are more dispersed and several locations near to the ground level which do not fail under isotropic condition

experience the triggering of relative RIS. A plausible explanation for this is the difference in the magnitudes of horizontal and vertical components of the seepage velocity due to anisotropy.

In the first heterogeneous case examined there is a zone of relatively high permeability, as shown in the inset of Figure 21. In this figure are also shown the predictions of the model for the heterogeneous and homogeneous cases. The presence of the zone of high permeability manifests itself by smaller number of triggering of relative RIS as compared to homogeneous case in the early stages of the FH and larger number activities than the homogeneous case during later time. This can be attributed to the fact that the high permeable zone prevents upstream pressure build-ups until the pressure wave reaches to the downstream end of the zone. The inset of Figure 22 shows the location of the faults considered in the other two cases of heterogeneity. The comparison of both temporal distribution (Figure 22) and spatial distribution (Figure 23) of predicted relative RIS activities demonstrates the capability of the model to respond effectively to a local zone of weakness. As illustrated, the imprint of the fault closer to the reservoir, N-fault, is more pronounced than that of the fault further away, F-fault, on the spatial distribution of relative RIS activities. This may be explained by the fact that the magnitude of change in pressures decreases with increasing distance from the reservoir.

CONCLUSIONS

A new analytical model for reservoir induced seismicity has been presented. The theoretical investigation of the behaviour of a geomass, subjected to water level variations in a man-made reservoir, based on the predictions of the model explicitly indicated the following:

1. The water level variations in a reservoir change the existing stress regime in a geomass. However, a local instability which thus may be acquired by these changes in both effective stresses and total stresses does not necessarily warrant triggering. The preloading state of stress determines the activation.
2. The temporal and spatial distributions of relative RIS activities are closely related to the filling
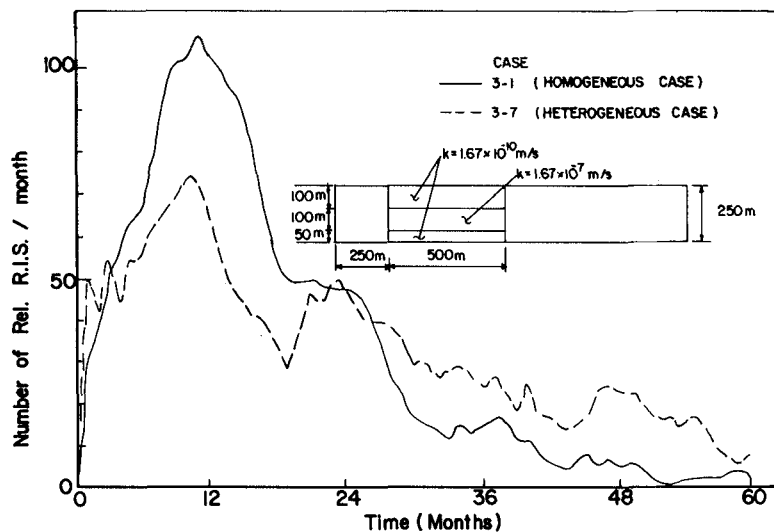

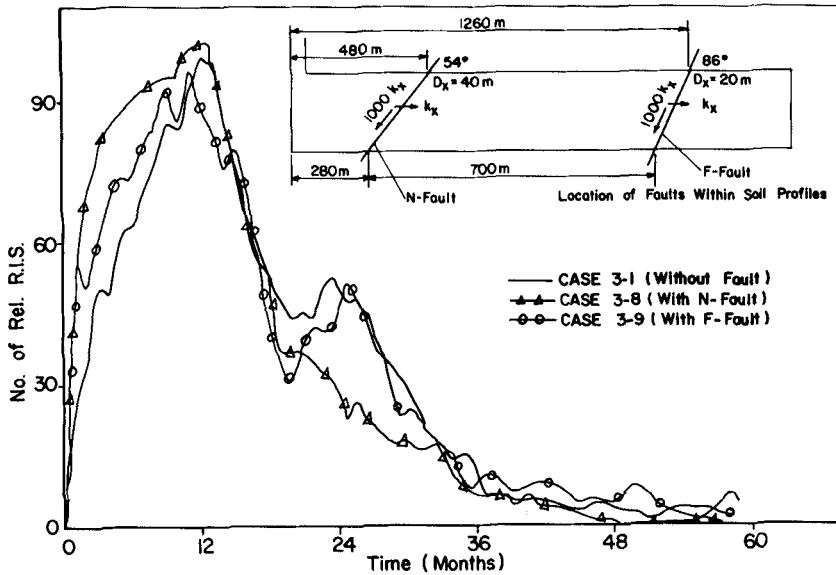Figure 21. Effect of heterogeneity: permeability

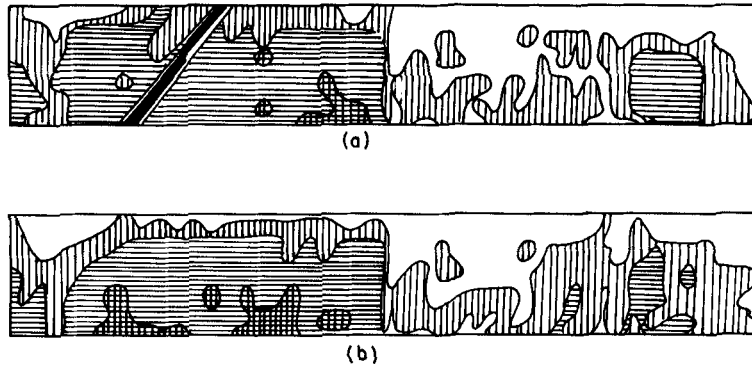Figure 22. Effect of heterogeneity: presence of faults

Figure 23. Spatial distribution of total number of relative RIS activities during first 60 months period: (a) N-fault and (b) F-fault (legend same as in Figure 20)

history. Both the rate of change of water level in the reservoir and the maximum water level attained are two major parameters shaping up these distributions.

3. Seismicity is also dependent on the strength and stiffness of the rock mass. The higher the strength and/or stiffness, the less the likelihood of triggering of relative RIS.

4. With decreasing permeability, the total number of relative RIS activities decreases and the time to maximum frequency of occurrence increases.

The presented model, contrary to Snow's model, predicts that the RIS may occur even at low K_0 value, provided that the pore pressure build-up is high. But the model, like Snow's model, predicts that the RIS is most likely to occur outside the periphery of the reservoir in two-

dimensional cases. The vertical load due to the water of the reservoir acts as a stabilizing force and prevents RIS from occurring. This also agrees with the observations at Koyna, Kremasta and other places. In all these cases the epicentres were found to be located at relatively shallow depth and initially far away from the reservoir.

Furthermore, the model is capable of simulating stabilization of the rock–reservoir system after a period of activities that follow the initial stage of reservoir water level variations. The model is also capable of responding effectively to some site-specific attributes such as local zones of weakness and anisotropy.

The development of the model is not yet complete. Several improvements can and are being implemented. A simple laboratory experiment is also being designed to verify the model quantitatively.

REFERENCES

1. D. R. Packer, L. S. Cluff, P. L. Knuepher and R. J. Withers, 'Study of reservoir induced seismicity', Final Technical Report on U.S.G.S. Contract No. 14-08-0001-16809 (1979).
2. H. K. Gupta et al. 'Some discriminatory characteristics of earthquakes near the Kariba, Kremasta, and Koyna artificial lakes', Bull. Seismol. Soc. Am. 62(2), 493–507 (1972).
3. H. K. Gupta et al., 'Common features of the reservoir-associated seismic activities', Bull. Seismol. Soc. Am., 62(2), 481–492 (1972).
4. T. Hagiwara and M. Ohtake, 'Seismic activity associated with the filling of the reservoir behind the Kurobe Dam, Japan, 1963–1970', Tectonophys. 15, 241–254 (1972).
5. D. W. Simpson and S. Kh. Negamatullaev, 'Induced seismicity at Nurek Reservoir, Tadjikistan, USSR', Lamont–Doherty Geological Observatory Contract No. 0000 (submitted to Bull. Seismol. Soc. Am.) (1980).
6. T. Vladut, 'Geotechnical aspects of the hazards of induced seismicity of water storage', 35th Canadian Geotech. Conf., Calgary, pp. 318–326 (1982).
7. D. I. Gough and W. I. Gough, 'Stress and deflection in the lithosphere near Lake Kariba—I', Geophys. J. Roy. Astronom. Soc., 21, 65–78 (1970).
8. D. I. Gough and W. I. Gough, 'Load induced earthquakes at Lake Kariba—II', Geophys. J. Roy. Astron. Soc., 21, 79–101 (1970).
9. T. Lee, 'A method for computing the deformation of the crust caused by the filling of large lakes', Bull. Seismol. Soc. Am., 62, 1597–1610 (1972).
10. E. Nyland and R. J. Withers, 'A fast method for computing load induced stress in the earth', Geophys. J. Roy. Astronom. Soc., 44, 689–698 (1976).
11. M. L. Bell and A. Nur, 'Strength changes due to reservoir induced pressure and stresses and applications to Lake Oroville', J. Geophys. Res., 83, 4469–4483 (1978).
12. M. A. Biot, 'General theory for three-dimensional consolidation', J. Appl. Phys., 12, 155–164 (1941).
13. R. J. Withers, 'Seismicity and stress determination at man-made lakes', Ph.D. dissert., Univ. of Alberta (unpublished) (1977).
14. A. M. Ger and S. K. Saxena, 'Reservoir induced seismicity: assessment of a mathematical model', 5th Int. Conf. on Numerical Methods in Geomechanics, Nagoya, Japan (1985).
15. S. K. Saxena, 'Induced seismicity—an engineering overview', Int. Conf. Geotechnical and Environmental Aspects of Geopressure Energy, Georgia, pp. 165–180 (1980).
16. D. T. Snow, 'On the determination of Poisson's ratio of large rock masses', Final Report on U.S.C.G. Contract No. 14-08-0001-12286 (1972).
17. D. T. Snow, 'Rock fracture spacings, openings and porosities', J. Soil Mech. Found. Div., A.S.C.E., pp. 73–91 (1968).
18. R. J. M. DeWiest, Flow Through Porous Media, Academic Press, New York, 1969.
19. T. H. Wu, Soil Mechanics, Allyn and Bacon Inc., Boston, 1967.
20. H. S. Carslaw and J. C. Jaeger, Conduction of Heat in Solids, Oxford University Press, London, 1978.
21. D. A. Howells, 'The time for a significant change of pore pressure', Eng. Geol., 8, 135–138 (1974).
22. S. K. Guha et al., 'Probable risk estimation due to reservoir induced seismicity, dams and earthquake', Proc. Conf. Inst. Civ. Eng., London, pp. 297–305 (Oct. 1980).
23. G. F. Pinder and W. G. Gray, Finite Element Simulation of Surface and Subsurface Hydrology, Academic Press, New York, 1982.
24. S. K. Saxena and A. Sengupta, 'Reservoir induced seismicity: a new model', Report No. IIT-CE-85-03, Illinois Inst. of Technology, Chicago (1985).
25. A. Sengupta, 'Reservoir induced seismicity: application of a new model', thesis submitted for the partial fulfilment of the Master of Science degree in Civil Engineering, Illinois Inst. of Technology, Chicago (1985).
26. O. C. Zienkiewicz, The Finite Element Method, McGraw-Hill, London, 1982.